Short Article

Developmental Cell

Vitamin D Stimulates Cardiomyocyte Proliferation and Controls Organ Size and Regeneration in Zebrafish

Graphical Abstract

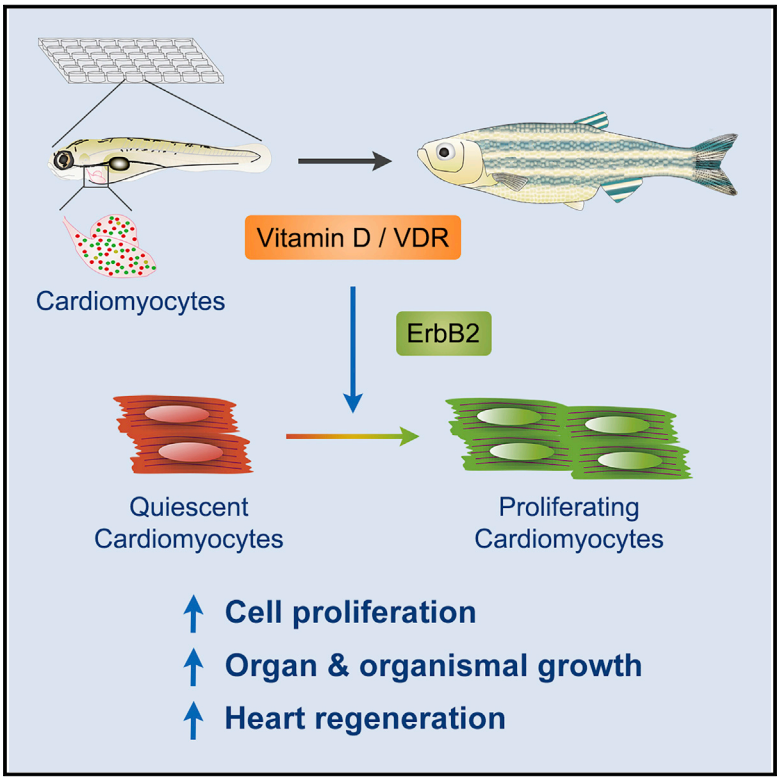

Authors

Yanchao Han, Anzhi Chen, Kfir-Baruch Umansky, ..., Ben D. Cox, Eldad Tzahor, Kenneth D. Poss

Correspondence

kenneth.poss@duke.edu

In Brief

By chemical screening, Han et al. find that vitamin D promotes cardiomyocyte proliferation during tissue growth, homeostasis, and injury-induced regeneration in zebrafish. Intact ErbB2 signaling is required for vitamin D's effects. In addition, vitamin D has broad and potent mitogenic effects on a variety of cell types across different tissues.

Highlights

- Vitamin D activates cardiomyocyte proliferation in several contexts in zebrafish
- Vitamin D controls growth rate and cycling in a wide range of adult cells
- Tissue-specific modulation of vitamin D activity controls cardiac size
- ErbB2 inhibition blunts vitamin D-induced cell proliferation

Han et al., 2019, Developmental Cell *48*, 1–11
March 25, 2019
https://doi.org/10.1016/j.devcel.2019.01.001

CellPress

Please cite this article in press as: Han et al., Vitamin D Stimulates Cardiomyocyte Proliferation and Controls Organ Size and Regeneration in Zebrafish, Developmental Cell (2019), https://doi.org/10.1016/j.devcel.2019.01.001

Developmental Cell
Short Article

Vitamin D Stimulates Cardiomyocyte Proliferation and Controls Organ Size and Regeneration in Zebrafish

Yanchao Han,[1,2] Anzhi Chen,[1,2] Kfir-Baruch Umansky,[3] Kelsey A. Oonk,[1,2] Wen-Yee Choi,[1] Amy L. Dickson,[1,2] Jianhong Ou,[1,2] Valentina Cigliola,[1,2] Oren Yifa,[3] Jingli Cao,[1,2] Valerie A. Tornini,[1,2] Ben D. Cox,[1,2] Eldad Tzahor,[3] and Kenneth D. Poss[1,2,4,*]

[1]Department of Cell Biology, Duke University Medical Center, Durham, NC 27710, USA
[2]Regeneration Next, Duke University, Durham, NC 27710, USA
[3]Department of Molecular Cell Biology, Weizmann Institute of Science, Rehovot 76100, Israel
[4]Lead Contact
*Correspondence: kenneth.poss@duke.edu
https://doi.org/10.1016/j.devcel.2019.01.001

SUMMARY

Attaining proper organ size during development and regeneration hinges on the activity of mitogenic factors. Here, we performed a large-scale chemical screen in embryonic zebrafish to identify cardiomyocyte mitogens. Although commonly considered anti-proliferative, vitamin D analogs like alfacalcidol had rapid, potent mitogenic effects on embryonic and adult cardiomyocytes *in vivo*. Moreover, pharmacologic or genetic manipulation of vitamin D signaling controlled proliferation in multiple adult cell types and dictated growth rates in embryonic and juvenile zebrafish. Tissue-specific modulation of vitamin D receptor (VDR) signaling had organ-restricted effects, with cardiac VDR activation causing cardiomegaly. Alfacalcidol enhanced the regenerative response of injured zebrafish hearts, whereas VDR blockade inhibited regeneration. Alfacalcidol activated cardiac expression of genes associated with ErbB2 signaling, while ErbB2 inhibition blunted its effects on cell proliferation. Our findings identify vitamin D as mitogenic for cardiomyocytes and other cell types in zebrafish and indicate a mechanism to regulate organ size and regeneration.

INTRODUCTION

Adult mammalian cardiomyocytes (CMs) can renew at a limited rate (Bergmann et al., 2009; Bergmann et al., 2015), yet there is minimal regeneration of lost CMs after myocardial infarction (MI). Adult zebrafish and neonatal mice or swine can regenerate heart muscle lost to severe trauma through dedifferentiation and proliferation of spared CMs (Jopling et al., 2010; Kikuchi et al., 2010; Porrello et al., 2011; Poss et al., 2002; Ye et al., 2018; Zhu et al., 2018). Recent reports indicate that forced expression of cyclins and/or cyclin-dependent kinases (CDKs) can activate spared CMs to re-enter cell cycle and improve heart function after injury (Hassink et al., 2008; Mohamed et al., 2018). Additional genetic factors have been implicated in promoting CM proliferation in various contexts, including Neuregulin1/ErbB2 (Bersell et al., 2009; D'Uva et al., 2015; Gemberling et al., 2015), and YAP/TAZ transcription factors, which are normally restrained by Hippo in CMs (Heallen et al., 2013; von Gise et al., 2012; Xin et al., 2013). Discovery of new influences that regulate CM proliferation can illuminate how and why heart regeneration occurs, and how to trigger cardiogenesis effectively after MI.

Chemical screening is a powerful technique to discover biological regulators. The zebrafish has been widely used for high-throughput chemical screening, owing to its small size, transparency, high fecundity, and rapid development. To monitor CM proliferation in live zebrafish embryos, we recently generated fluorescent ubiquitin-based cell cycle indicator (FUCCI) dual transgenes under control of the zebrafish *cmlc2* promoter (*cmlc2:FUCCI*) (Choi et al., 2013). In this system, Venus-hGeminin fusion protein accumulates at S/G2/M phases in CMs and degrades quickly afterwards, whereas mCherry-zCdt1 fusion protein is degraded at S/G2/M and accumulates during G1/G0 (Sakaue-Sawano et al., 2008). Thus, by direct visual inspection in live zebrafish, one can readily track all or most proliferating CMs and the effects of experimental manipulations on cardiogenesis.

Here, we employed the FUCCI detection system in a large-scale chemical screen for compounds that impact CM proliferation in zebrafish embryos. Unexpectedly, we found that vitamin D analogs, commonly considered to be anti-proliferative influences in mammalian cells, are potent cardiogenic factors in both embryonic and adult zebrafish. We show that increased vitamin D signaling enhances cell proliferation in many cell types and contexts, including cardiac regeneration. Manipulation of vitamin D signaling in growing zebrafish has major effects on animal size, and locally dysregulating the pathway in specific cell types can reduce or increase cardiac size. Transcriptome profiling and pharmacological perturbation implicated ErbB2 signaling as a key growth network regulated by vitamin D. Our results reveal vitamin D signaling as a profound mitogenic influence in a vertebrate model system.

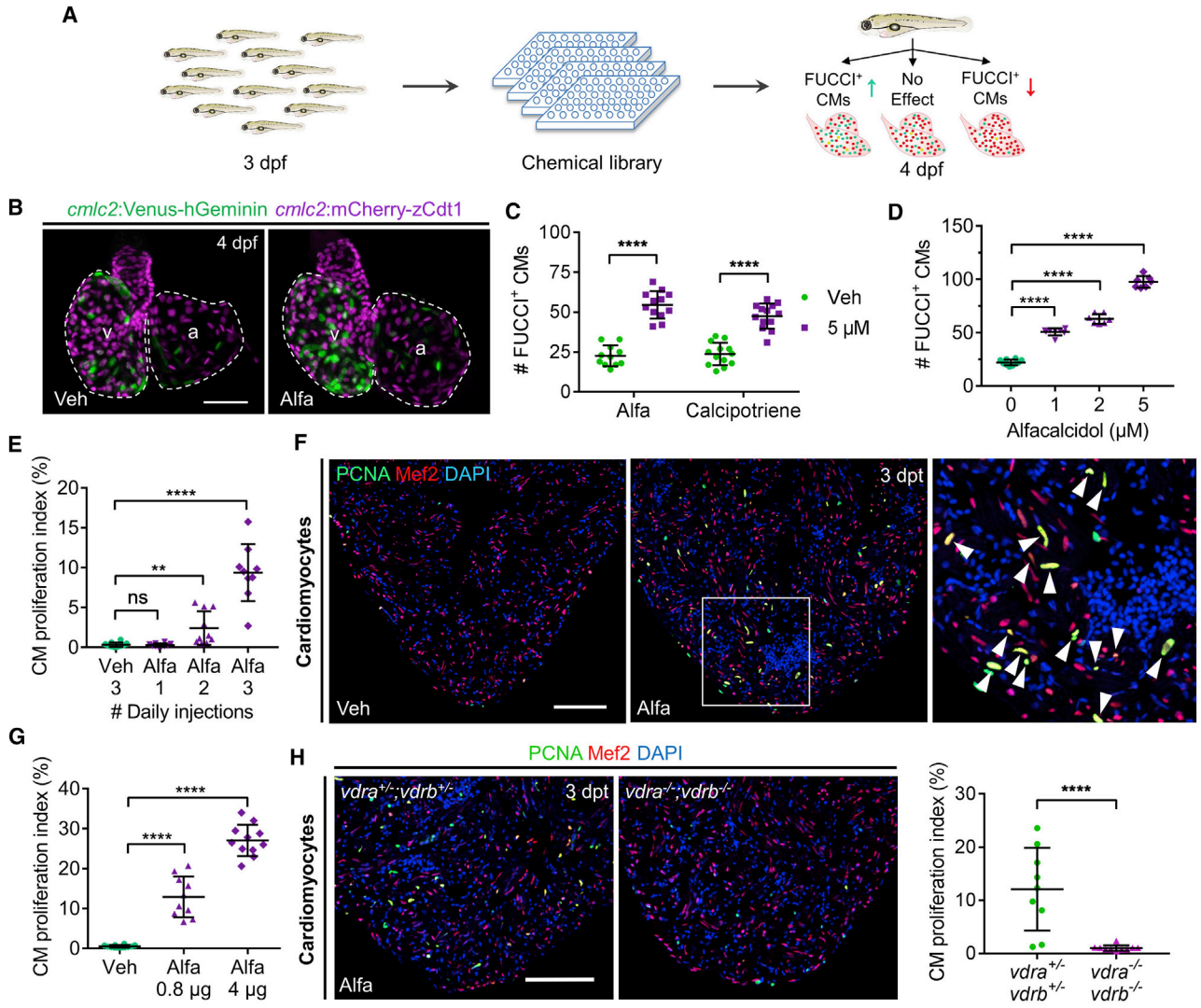

Figure 1. Vitamin D Analogs Promote Cardiomyocyte Proliferation in Zebrafish

(A) Cartoon schematic of *in vivo* chemical screen for regulators of CM proliferation using *cmlc2:FUCCI* zebrafish embryos. dpf, days post-fertilization.

(B) Maximum intensity projection (MIP) images of dissected *cmlc2:FUCCI* hearts. Veh, vehicle; v, ventricle; a, atrium. Scale bar, 50 μm.

(C) Quantification of FUCCI$^+$ CMs after 24-h treatment. Mean ± SD, Mann-Whitney test and Student's t test. ****p < 0.0001. n = 11–13.

(D) Quantification of FUCCI$^+$ CMs after 24-h treatment. Mean ± SD, Mann-Whitney test and Student's t test. n = 7–10.

(E) Quantification of adult ventricular CM proliferation indices. Mean ± SD, Mann-Whitney test and Student's t test. ns, not significant; **p < 0.01. n = 9–10.

(F) Representative images of PCNA/Mef2 staining quantified in (E). Boxed area is enlarged on the right. Arrowheads indicate PCNA$^+$ CMs. dpt, days post-treatment. Scale bar, 100 μm.

(G) Ventricular CM proliferation indices of vehicle- or Alfa-injected adult zebrafish. Mean ± SD, Mann-Whitney test and Student's t test. n = 10–12.

(H) Representative images and quantification of ventricular PCNA/Mef2 staining. Mean ± SD, Mann-Whitney test. n = 9–10. Scale bar, 100 μm.

See also Figure S1; Table S1; and Video S1.

RESULTS

Chemical Screening Identifies Vitamin D Analogs as Activators of Embryonic Cardiomyocyte Proliferation

To discover compounds that regulate CM proliferation in zebrafish, we screened the Prestwick Chemical Library for effects on the number of Venus-hGeminin$^+$; mCherry-zCdt1$^-$ (FUCCI$^+$) CMs in *cmlc2:FUCCI* embryos after a 24-h treatment starting at 3 days post-fertilization (dpf) (Figure 1A). We found that 104 and 26 compounds from a total of 1,200 tested drugs increased or decreased the number of FUCCI$^+$ CMs, respectively (Figure S1A). Modulator classes include neurotransmission, steroid hormone effectors, antimicrobial influences, and ion channel regulators (Figure S1B; Table S1). Two out of the 18 hormone effectors, alfacalcidol (Alfa) and calcipotriene, are vitamin D analogs.

Vitamin D, widely studied for over 80 years, is a steroid prohormone that can be hydroxylated sequentially in the liver and kidney to yield the active hormone, ercalcitriol (D_2) or calcitriol (D_3), in vertebrates (Bikle, 2014). Alfa is a vitamin D analog that can be hydroxylated to form calcitriol directly in the liver

(Ringe and Schacht, 2007). The active hormones ercalcitriol and calcitriol can bind to vitamin D receptors (VDRs) and regulate downstream gene expression in target cells (Bikle, 2014). Notably, many studies have reported vitamin D analogs to have anti-proliferative effects in mammalian cells (Ma et al., 2016; Samuel and Sitrin, 2008), including cultured CMs (Hlaing et al., 2014; Nibbelink et al., 2007; O'Connell et al., 1997). In our screen, treatment with Alfa elevated the number of FUCCI^{+} CMs in live embryonic zebrafish by 141%, the largest increase among library compounds. Similarly, calcipotriene also increased FUCCI^{+} CMs by 100% (Figures 1B and 1C). In addition, both Alfa and calcitriol had dose-dependent effects on the number of FUCCI^{+} CMs. (Figures 1D and S1C). By contrast, treatment with the VDR-specific inhibitor PS121912 (Sidhu et al., 2014) caused a 39% reduction in the number of FUCCI^{+} CMs (Figure S1C). These findings indicate that vitamin D is a potent activator of CM proliferation in embryonic zebrafish.

Vitamin D Signaling Stimulates Cell Cycle Re-entry in Adult Cardiomyocytes and Other Cell Types

Adult zebrafish hearts are similar to adult mammalian hearts in that the majority of CMs are quiescent under normal conditions (Wills et al., 2008). To determine the potency of vitamin D in mature cardiac tissue, we injected Alfa intraperitoneally in adult zebrafish. One day after Alfa injection, CMs remained quiescent, with no significant difference in the percentage of CMs positive for the proliferation marker PCNA compared to vehicle-injected fish (Figure 1E). After two daily Alfa injections, the CM proliferation index increased moderately in 4 out of 10 animals (Figure 1E). By contrast, the CM proliferation indices of all animals rose in a dose-dependent manner after 3 daily Alfa injections, to an average index of 27% at the highest dose, a 50.9-fold increase over vehicle-injected controls (an average index of 0.52%) (Figures 1F and 1G). We found no evidence of enhanced apoptosis upon Alfa treatment that might indirectly lead to CM proliferation in adult hearts (data not shown).

To interrogate broader effects of vitamin D, we next asked whether Alfa injections increased indicators of proliferation in several additional adult zebrafish cell types. We found that Alfa boosted proliferation indices of non-muscular epicardial and endocardial cells of the heart by 26.6-fold and 4.7-fold, respectively (Figures S1D and S1E). In addition, Alfa enhanced the proliferation of adult liver cells, including hepatocytes by 9.0-fold and biliary duct cells by 4.0-fold (Figures S1F and S1G). Alfa also stimulated proliferation of dermal osteoblasts and basal epithelial cells in fins, corneal epithelial cells, and retinal cells (Figures S1H–S1J). Retinal cells in the ciliary marginal zone (CMZ), a dense region of progenitor cells, were more responsive to Alfa than mature cells (Figures S1H–S1J). Interestingly, a recent study reported that vitamin D signaling can promote hematopoietic progenitor cell proliferation in zebrafish (Cortes et al., 2016). Together, these findings indicate that vitamin D signaling is mitogenic for a wide spectrum of adult zebrafish cells.

To determine how cell cycle progression is affected, we imaged *tcf21:FUCCI* cardiac tissue explants treated with vehicle or calcitriol and cultured *ex vivo* for long time periods (Figure S1K; Video S1) (Cao et al., 2017). Compared to vehicle controls, the number of *tcf21*-expressing epicardial cells bypassing the G1 checkpoint and entering S phase (characterized by a red [false colored as magenta] to green conversion; Figure S1L) was increased by 79% on average over a 69-h period during continual calcitriol treatment (Figure S1N). The number of cells traversing the G2 checkpoint to M phase (characterized by breakdown of nuclear membrane and subsequent dispersal of the green signal; Figure S1M) was also increased but only by 14% (Figure S1O). These data suggest that the principal effect of vitamin D treatment is surpassing the G1 checkpoint to initiate the cell cycle.

Vitamin D Signaling Rapidly Accelerates Organismal Growth

Our results indicated that many zebrafish tissues respond to vitamin D treatment. To visualize vitamin D signaling activity in live zebrafish, we knocked in a monomeric EGFP-polyA (mGFP) cassette at the *cyp24a1* start codon. *cyp24a1* encodes a mitochondrial cytochrome P450 enzyme that catabolizes calcitriol to inactivate vitamin D signaling and is a direct downstream target gene of vitamin D signaling (Bikle, 2014). *cyp24a1*^{mGFP} embryos displayed conspicuous mGFP fluorescence in cardiac ventricles (Figure S2), indicating active vitamin D signaling during heart development. When incubated with Alfa, *cyp24a1*-driven mGFP expression was increased sharply throughout embryonic zebrafish tissues with the greatest enhancement in liver (Figure S2), validating this line as a reporter of embryonic vitamin D signaling levels.

To examine how vitamin D analogs affect organismal growth, we first tested if they increased embryonic cell proliferation and size. Indeed, Alfa treatments longer than 9 h elevated the number of cells positive for the mitotic marker phospho-Histone H3 (Figure 2A) throughout the trunks of 3 dpf embryos. Strikingly, we found that the total lengths of Alfa- or calcipotriene-treated embryos were increased by ~3% after treatment from 3 to 4 dpf over vehicle controls, representing a 43% (Alfa) or 30% (calcipotriene) faster growth rate during the 24-h treatment (Figure 2B). To test if vitamin D had effects on post-metamorphic growth, we treated 5 weeks post-fertilization (wpf) juvenile zebrafish with Alfa for 15 or 30 days. We found that Alfa-treated animals were 10% longer after 30 days of treatment, having grown substantially (33%) more than vehicle-treated clutch mates (Figures 2C and 2D). These data demonstrate that exogenous vitamin D is sufficient to accelerate zebrafish growth and boost animal size.

To examine how the size-enhancing effects of Alfa reflect endogenous roles, we disabled vitamin D signaling by multiple different ways. To deplete endogenous vitamin D metabolites, we generated transgenic *ubb:cyp24a1* zebrafish that constitutively express *cyp24a1* via the *ubiquitin* promoter (Mosimann et al., 2011) (Figure 2E). Total body lengths in two independent lines of *ubb:cyp24a1* animals were ~3% shorter than those of wild-type (WT) siblings at 4 dpf (Figure 2F) and 33% shorter at 5 wpf (line 2; Figure 2D). A low (10 nM) dose of Alfa was sufficient to rescue *cyp24a1*^{mGFP} expression and growth rate in *ubb:cyp24a1* animals (Figures 2C–2E), indicating that the transgene product had negligible toxicity and could be saturated by substrate. To genetically disable endogenous VDRs, we generated zebrafish containing mutations in *vdra* and *vdrb* using CRISPR/Cas9-based gene editing (Varshney et al., 2015). Knockdown of zebrafish *vdra* and *vdrb* using morpholino oligonucleotides was reported to cause pericardial edema (Kwon, 2016), although

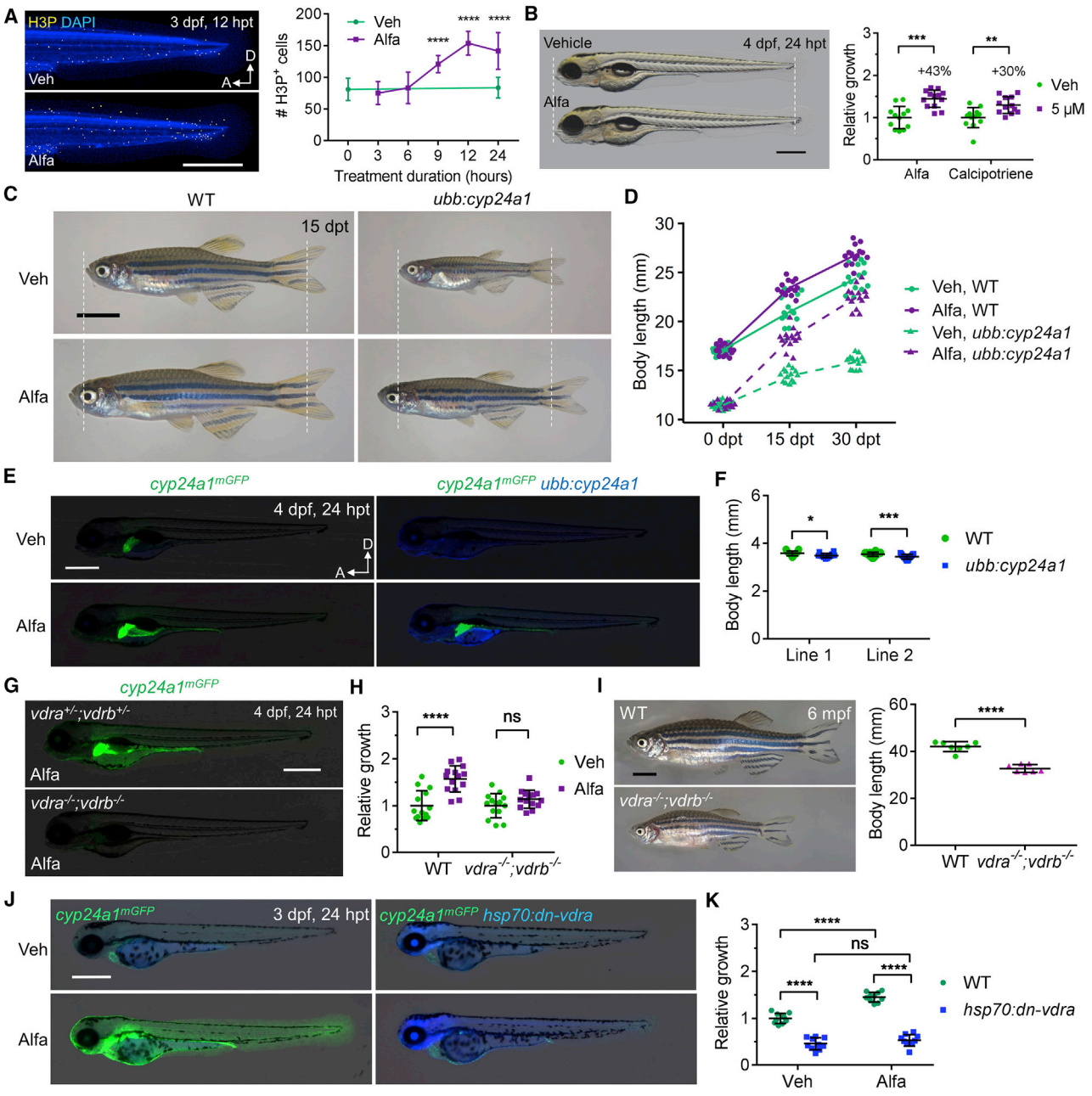

Figure 2. Vitamin D Signaling Enhances Organismal Size

(A) MIP images and quantification of H3P staining of 3 dpf embryos. hpt, hours post-treatment; H3P, phospho-Histone H3. Mean ± SD, Mann-Whitney test and Student's t test. ****p < 0.0001. n = 11–13. Scale bar, 500 μm.

(B) Example and quantification of 4 dpf zebrafish growth. Mean ± SD, Mann-Whitney test and Student's t test. **p < 0.01; ***p < 0.001. n = 12-14. Scale bar, 500 μm.

(C) Growth and rescue of 2 mpf juvenile wild-type (WT) and *ubb:cyp24a1* zebrafish. Scale bar, 4 mm.

(D) Quantification of zebrafish length before and after treatment. Mean ± SD. n = 14–15.

(E) mGFP and TagBFP expression in 4 dpf embryos treated with vehicle or 10 nM Alfa. Scale bar, 500 μm.

(F) Quantified body length of two independent *ubb:cyp24a1* lines and WT siblings at 4 dpf. Mean ± SD, Mann-Whitney test. *p < 0.05. n = 14–23.

(G) *cyp24a1*^{mGFP} expression in 1 μM Alfa-treated embryos.

(H) Quantification of relative growth of 4 dpf embryos treated with vehicle or Alfa for 24 h. Mean ± SD, Student's t test. n = 13.

(I) Representative images and body length quantification of 6 mpf zebrafish. mpf, months post-fertilization. Mean ± SD, Student's t test. n = 7. Scale bar, 5 mm.

(J) mGFP and TagBFP expression of 3 dpf embryos after a single heat-shock and 24-h drug treatment. Scale bar, 500 μm.

(K) Quantified relative growth of 4 dpf embryos after a heat shock and 24-h drug treatment. Mean ± SD, Student's t test. n = 10.

See also Figure S2.

we did not observe this phenotype in *vdra*$^{-/-}$; *vdrb*$^{-/-}$ mutants. Nevertheless, homozygous mutations in both *vdr* genes abolished *cyp24a1*^{mGFP} expression and rapid embryonic growth in response to Alfa treatment, indicating a genetic requirement for VDRs in this response (Figures 2G and 2H). Additionally, *vdra*$^{-/-}$; *vdrb*$^{-/-}$ mutant zebrafish were 22% smaller in length than WT siblings at 6 months post-fertilization (mpf) (Figure 2I). They also demonstrated no increase in the proliferative response of adult CMs after 3 daily Alfa injections, indicating a genetic requirement for VDRs in the mitogenic effects of Alfa (Figure 1H). To block VDR signaling in a conditional manner, we generated transgenic lines enabling heat shock (*hsp70* promoter)-inducible expression of a dominant negative *vdra* (*dn-vdra*) cassette throughout the animal. Heat-shock treatment at 3 dpf inhibited growth in *hsp70:dn-vdra* embryos by 54% versus controls over the following 24 h, and it eliminated the growth response to Alfa (Figures 2J and 2K). Collectively, these findings identify vitamin D signaling as an endogenous pathway that controls organ and organismal size in zebrafish.

Vitamin D Regulates Organ Size through Tissue-Intrinsic Signaling

As a circulating nutrient, vitamin D could influence cell proliferation directly by VDR signaling in the organs itself, and/or through a relay mechanism that relies on VDR signaling in other organs. To distinguish such mechanisms in CMs, we generated transgenic lines that express *dn-vdra* or constitutively active *vdra* (*ca-vdra*) via the *cmlc2* promoter. When crossed to *cyp24a1*^{mGFP} animals, *cmlc2:dn-vdra* zebrafish displayed little or no cardiac mGFP fluorescence and unchanged fluorescence elsewhere (Figures 3A and S3A), indicating specific inhibition of cardiac VDR signaling. By contrast, *cmlc2:ca-vdra*; *cyp24a1*^{mGFP} animals had sharply elevated mGFP fluorescence in both cardiac chambers and unchanged mGFP fluorescence elsewhere (Figures 3B and S3B), indicating targeted enhancement of cardiac VDR signaling. To assess effects of these transgenes on CM proliferation, we examined them in the *cmlc2:FUCCI* or *cmlc2:H2A-EGFP* (labeling all CM nuclei) backgrounds. *cmlc2:dn-vdra* reduced the average number of FUCCI^{+} CMs by 63% at 4 dpf, yielding hearts with 31% fewer total CMs on average, whereas *cmlc2:ca-vdra* increased the number of FUCCI^{+} CMs by 171% and the total number of CMs by 74% (Figures 3C, 3D, S3C, and S3D). Notably, juvenile *cmlc2:ca-vdra* animals displayed overt cardiomegaly, with massive hearts dwarfing those of clutch mates by 1 mpf (Figures 3E and 3F). Ventricular walls were dysmorphic and thickened (Figure S3E), and we cannot rule out the possibility of direct or indirect contributions through cell hypertrophy during these events. By contrast, assessment of heart-to-body size ratios in juvenile *cmlc2:dn-vdra* animals versus WT siblings indicated a 27% smaller ratio during VDR inhibition (Figure S3F). Thus, cardiac-intrinsic changes in VDR signaling are sufficient to regulate CM proliferation and heart size.

To supplement these experiments, we examined whether modulation of VDR signaling in a distant organ, the liver, influenced cardiac cell proliferation or size. Among all embryonic tissues, we noted that liver displayed the sharpest increase in *cyp24a1*^{mGFP}-directed fluorescence in response to Alfa treatment (Figure S2). New transgenic lines expressing *dn-vdra* or *ca-vdra* driven by *fabp10a* regulatory sequences in hepatocytes directionally controlled hepatic *cyp24a1* reporter fluorescence in zebrafish (Figure S3G). In these animals, embryonic hearts had normal numbers of FUCCI^{+} CMs and were of a similar size as those of clutch mates (Figures S3H and S3I). Interestingly, whereas the hearts of juvenile *fabp10a:ca-vdra* zebrafish appeared normal, their livers were grossly enlarged (Figure 3G). Taken together, our data indicate that vitamin D dictates CM proliferation and controls heart size in growing zebrafish through intrinsic signaling and that this principle can extend to other organs.

Vitamin D Signaling Regulates Heart Regeneration

Zebrafish possess a wide range of tissues with an elevated capacity to regenerate after major injury. In uninjured hearts, sparse *cyp24a1*^{mGFP} fluorescence was detectable in CMs and other cardiac cells. This fluorescence became more prominent in ventricles injured by partial resection or induced CM ablation (Figures S3J and S3K) although cardiac *cyp24a1*^{mGFP} expression patterns and levels varied among animals. To test whether vitamin D treatment augments proliferation of CMs during heart regeneration, we partially resected adult zebrafish ventricles and injected Alfa at 6 days post-resection (dpa), 1 day before harvesting tissues at 7 dpa. By contrast with CMs of uninjured animals that have little or no response to a single Alfa injection (Figure 1E), a single treatment was sufficient to increase CM proliferation indices by 41% in regenerating hearts (Figures 3H and 3I). This result is consistent with the notion that vitamin D is more potent in CMs that are sensitized by injury or primed for regeneration programs. VDR inhibition by heat shock-induced *dn-vdra* transgene expression from 6 to 7 dpa had an opposite effect, reducing CM proliferation by 69% (Figure S3L). Moreover, sustained expression of *dn-vdra* after 6 dpa blocked heart regeneration, with ventricles retaining large scars in the injury sites at 50 dpa (Figures 3J–3L and S3N). Thus, vitamin D signaling is essential for normal heart regeneration.

Stimulation of heart regeneration in mammals by secreted factors may be more complex than in zebrafish, as mammalian adult CMs have a lower proliferative capacity and/or more hurdles to division like polyploidy (Gonzalez-Rosa et al., 2018; Patterson et al., 2017). Vitamin D signaling has been reported to protect mouse CMs from pathological hypertrophy by regulation of calcium handling (Chen et al., 2011; Choudhury et al., 2014; Ford et al., 2018), but we have identified no clear evidence from published literature for hyperplastic effects in mammalian hearts. To examine potential effects on cultured mouse P7 CMs, we treated with different concentrations of calcitriol and examined the expression of the proliferation marker Ki67 after 3 days. The frequency of Ki67^{+} CMs was increased in a dose-dependent manner (Figure S3M), suggesting that vitamin D supplementation is sufficient to induce mouse CM cycling *in vitro*.

Mitogenic Effects of Vitamin D Require ErbB2 Signaling

Vitamin D has been reported to regulate calcium homeostasis, vasculogenesis, and fatty acid oxidation in embryonic zebrafish (Lin et al., 2012; Merrigan and Kennedy, 2017; Peng et al., 2017), and VDR transcriptional targets are reported to be species and context dependent (Campbell and Trump, 2017). To identify downstream genes and pathways underlying vitamin D-induced

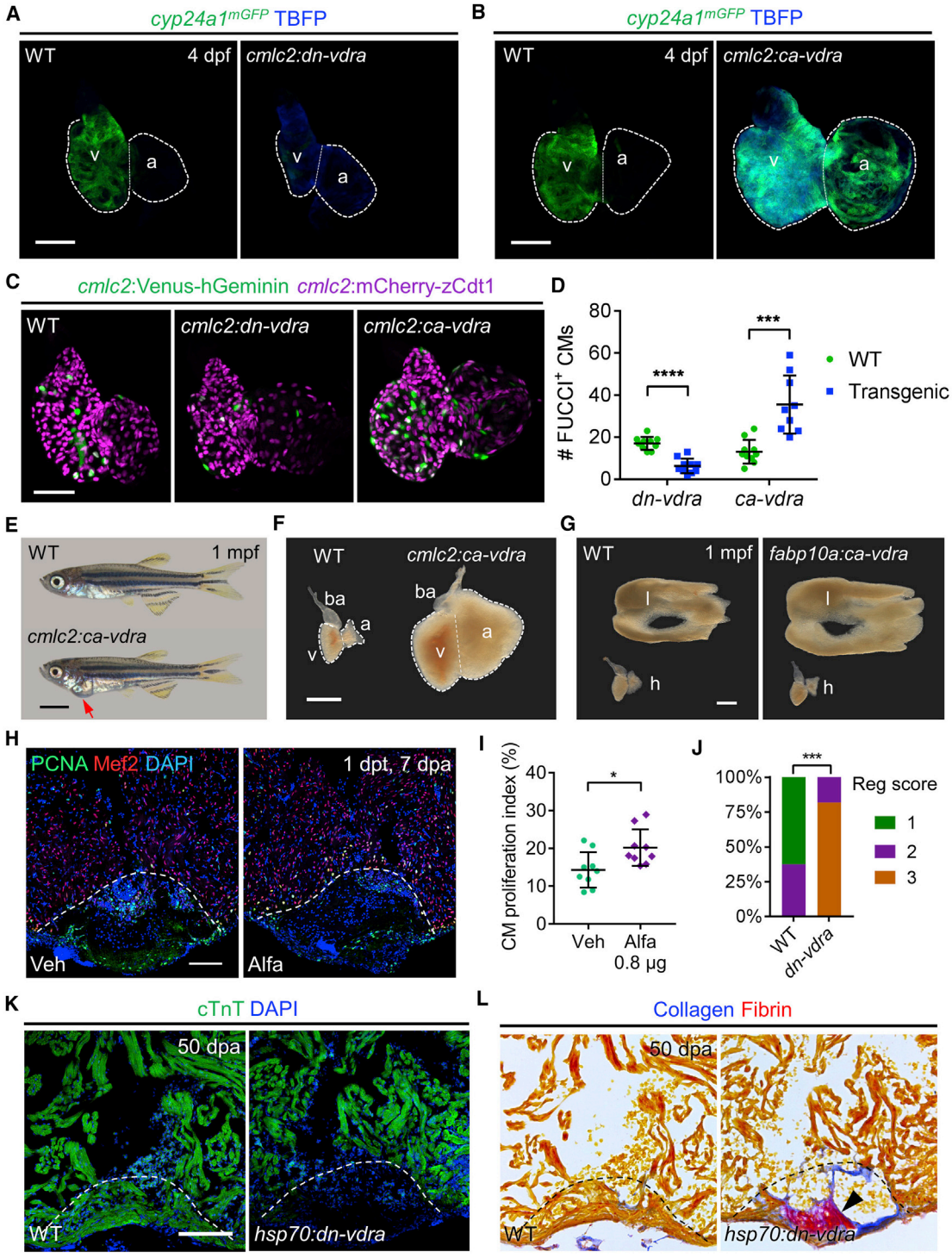

Figure 3. Tissue-Intrinsic Effects of Vitamin D Signaling and Impact on Heart Regeneration

(A) MIP images of *cyp24a1*^{mGFP} expression in dissected hearts. Scale bar, 50 µm.

(B) MIP images of *cyp24a1*^{mGFP} expression in dissected hearts. Scale bar, 50 µm.

(C) MIP images of dissected *cmlc2:FUCCI* hearts in indicated transgenic backgrounds. Scale bar, 50 µm.

(D) Quantification of FUCCI^{+} CMs in (C). Mean ± SD, Mann-Whitney test and Student's t test. ***p 0.001; ****p < 0.0001. n = 9–10.

(E) Examples of 1 mpf *cmlc2:ca-vdra* and WT zebrafish. Red arrow indicates gross pericardial enlargement caused by cardiomegaly in *cmlc2:ca-vdra* zebrafish. Scale bar, 2 mm.

(F) Darkfield images of dissected 1 mpf hearts. a, atrium; ba, bulbus arteriosus; v, ventricle. Scale bar, 500 µm.

(G) Darkfield images of dissected livers (l) and hearts (h) from 1 mpf zebrafish. Scale bar, 500 µm.

(legend continued on next page)

cell proliferation, we sequenced cardiac transcriptomes of zebrafish injected with vehicle or Alfa. Among 14,962 recovered genes, 767 showed >2-fold higher levels with Alfa treatment, whereas levels of 495 genes were reduced by 50% or more (Table S2A). Functional clustering analysis indicated that levels of many genes involved in cell-cycle regulation and DNA repair were increased, including *cyclins (A2/B1/B2/B3/D2/E1/E2/F/J)*, *cdks (1/2/6)*, *e2fs (1/3/4/7/8)*, and *mcms (2/3/4/5/6/7/8/9/10)* (Figure 4A; Table S2B), consistent with the observed effects on cell proliferation and G1 checkpoint release. In addition, genes involved in metabolic pathways like steroid, nucleotide, and amino acid biosynthesis and/or degradation were enriched upon Alfa injection (Table S2B), although we detected no common metabolite level changes induced by Alfa among adult hearts, livers, and whole embryos by metabolomic analysis (Figure S4A; Table S3).

To identify common upstream regulators of differentially expressed genes, we analyzed RNA sequencing (RNA-seq) datasets using Ingenuity Pathway Analysis (IPA) software (Kramer et al., 2014). From this analysis, the EGF receptor family member ErbB2 emerged as the signaling effector with the highest enrichment and activation scores (Figure 4B; Table S2C); 135 ErbB2-associated genes were differentially expressed (Figure S4B; Table S2D). Notably, ErbB2 and one of its activating ligands Nrg1 have been functionally implicated as CM mitogens in zebrafish and mice (Bersell et al., 2009; D'Uva et al., 2015; Gemberling et al., 2015), with Nrg1 overexpression able to boost CM proliferation in the absence of injury in adult zebrafish (Gemberling et al., 2015). Also, daily calcitriol administration to rats over a period of 6 weeks was associated with modest cardiac increases in Nrg1 and ErbB2 proteins (Dang et al., 2016). We performed quantitative PCR for 19 ligand, receptor, and target genes, finding 9 of which had at least 2-fold increases in hearts of Alfa-treated animals (Figure S4C). To test if ErbB2 signaling is required for the effects of vitamin D signaling, we treated zebrafish embryos or adults with Alfa and the commonly used ErbB2 inhibitor, AG1478. AG1478 reduced CM proliferation in *cmlc2:FUCCI* embryos, and it abolished Alfa stimulation of CM proliferation (Figures 4C and 4D). Moreover, AG1478 blocked the increase in CM proliferation caused by cardiac expression of a *ca-vdra* transgene (Figures 4E and 4F). In addition, AG1478 inhibited Alfa-induced osteoblast proliferation (Figure S4D) in adults and Alfa-induced growth in zebrafish embryos (Figures S4E and S4F). Notably, AG1478 incubation reduced the CM proliferation index in Alfa-injected adult zebrafish to 0.6%, comparable to the index of vehicle-injected zebrafish and ~94% lower than that of animals treated with Alfa alone in these experiments (Figures 4G and 4H). Taken together, these data indicate that the mitogenic and growth-promoting effects of vitamin D on zebrafish CMs and other cell types require ErbB2 signaling.

DISCUSSION

Modulating VDR activity selectively in zebrafish CMs or hepatocytes is sufficient to control heart or liver size, respectively. This finding indicates that vitamin D effects do not require signaling in distant tissues, though it does not rule out possible influences of systemic signaling. It is also possible that local relays involving secreted mitogenic factors or cell-cell interactions within these tissues are activated by vitamin D signaling, rather than a formal cell-autonomous effect. Because vitamin D is a circulating factor, the effects we report make it a candidate signal to synchronize growth among different tissues in growing zebrafish—that is, to achieve proportional growth. This synchrony was maintained in whole-animal manipulation of vitamin D signaling, but cardiac or hepatic growth no longer tracked with animal growth when VDR activity was selectively manipulated. How vitamin D modulates intracellular ErbB2 signaling requires further investigation; one possible mechanism is by sensitizing cells to activation of this pathway. Thousands of VDR-binding elements exist throughout vertebrate genomes (Carlberg and Seuter, 2009), and systematic methods to identify VDR interactomes in different developmental contexts should be useful to illuminate key mechanisms.

The majority of studies assessing proliferation of mammalian cells in response to vitamin D have reported inhibitory effects, most notably in tumor cells (Ma et al., 2016; Samuel and Sitrin, 2008). Previous studies of mammalian CMs have suggested that VDR signaling regulates CM differentiation and hypertrophy and represses CM cycling (Hlaing et al., 2014; Nibbelink et al., 2007; O'Connell et al., 1997), whereas our data indicate that elevated vitamin D concentrations can increase cycling. The effects of vitamin D on cell proliferation are likely context dependent and/or concentration dependent and are affected by species' distinct VDR target gene repertoires and collaborating regulatory sequences.

Vitamin D deficiency has been associated with various cardiovascular diseases, and VDR signaling has been reported to protect ischemic myocardium through anti-inflammatory, anti-fibrotic, and anti-apoptotic mechanisms (Bae et al., 1985; Chen et al., 2011; Simpson et al., 2007; Yao et al., 2015). Vitamin D and its analogs have been widely used to prevent and/or treat many diseases, including rickets, osteoporosis, osteomalacia, hypocalcemia, hypertension, hypercholesterolemia, hyperparathyroidism, diabetes, and psoriasis. Yet, excessive vitamin D can lead to hypercalcemia and vascular calcification (Pilz et al., 2016; Tebben et al., 2016), challenging the use of systemic vitamin D administration to enhance tissue regeneration. Our results indicate that modulation of vitamin D signaling or sensitivity, e.g., targeted or tailored mechanisms to increase VDR activation in specific cell types without impacting physiological calcium

(H) Examples of Mef2/PCNA staining of 7 dpa hearts after a single injection. Dashed lines represent amputation planes. Scale bar, 100 μm.
(I) Quantification of CM proliferation indices in (H). Mean ± SD, Mann-Whitney test. *$p < 0.05$. n = 9.
(J) Quantified heart regeneration scores of WT or *hsp70:dn-vdra(dn-vdra)* zebrafish given daily heat shocks from 6 to 50 dpa. Regeneration scores (reg scores) indicate vigorous regeneration (1), partial regeneration (2), or blocked regeneration (3), as shown in Figure S3N. Two-tailed Fisher's exact test. ***$p < 0.001$. n = 8–11.
(K) Representative images of cTnT staining at 50 dpa, after daily heat shock from 6 dpa. Scale bar, 100 μm.
(L) Representative images of AFOG stains to indicate fibrin (red) and collagen (blue) within the same hearts in (K). Arrowhead indicates scar tissue.
See also Figure S3.

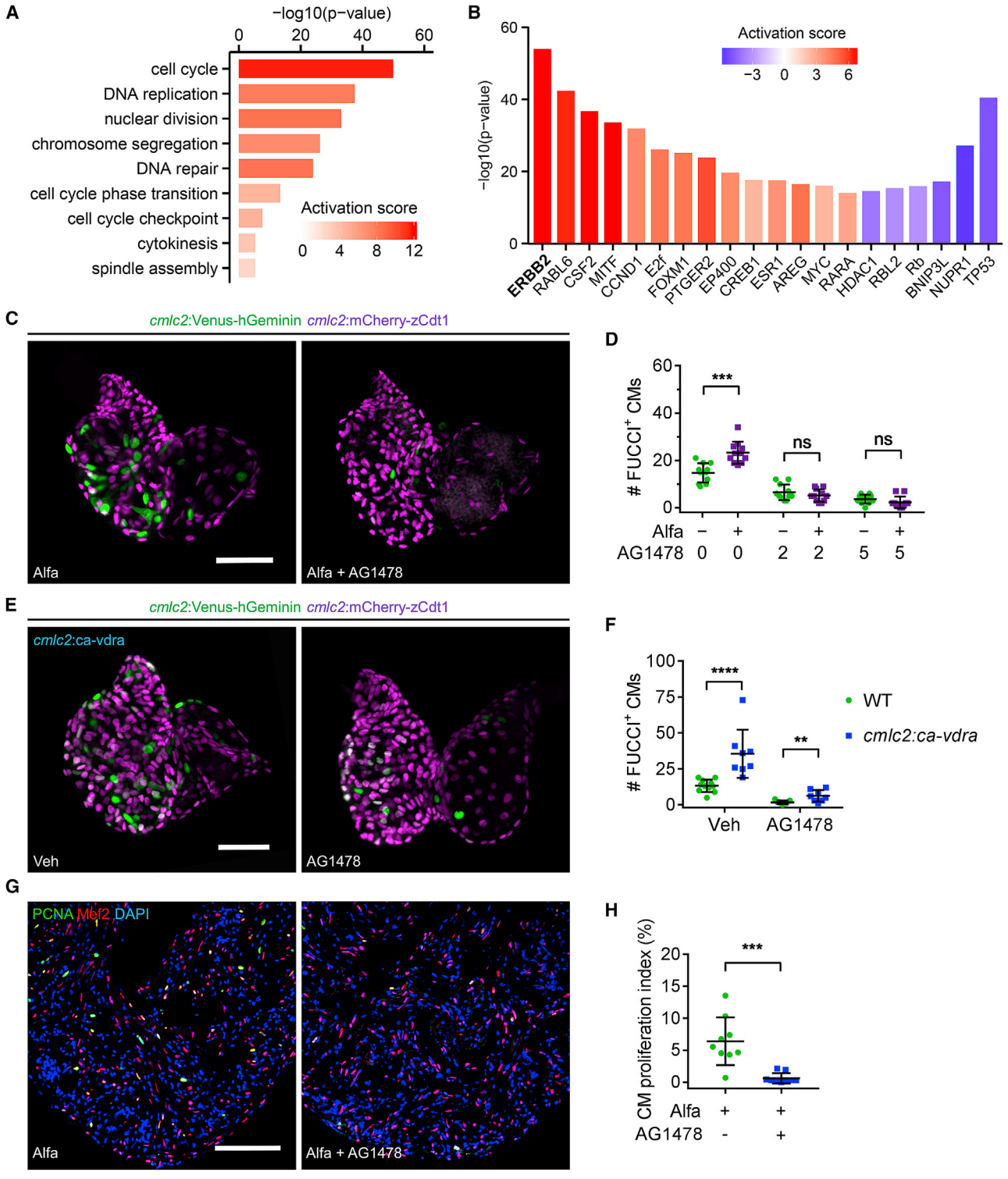

Figure 4. ErbB2 Blockade Inhibits Vitamin D-Induced Cardiomyocyte Proliferation

(A) Selected functional cluster enrichment of differentially expressed genes. The activation score infers the activation score of the corresponding process.

(B) Selected common upstream regulators of differentially expressed genes in adult hearts after three Alfa injections. The p value measures the statistical significance of the overlap between differentially expressed genes and the genes under predicted control of a regulator, and the activation score infers the activation state and score of a regulator, either activating (positive) or inhibiting (negative).

(C) MIP images of dissected 4 dpf *cmlc2:FUCCI* hearts after 24-h treatment. Scale bar, 50 μm.

(legend continued on next page)

handling, can be incorporated into potential methods to boost regeneration of the injured heart or other tissues.

STAR★METHODS

Detailed methods are provided in the online version of this paper and include the following:

- KEY RESOURCES TABLE
- CONTACT FOR REAGENT AND RESOURCE SHARING
- EXPERIMENTAL MODEL AND SUBJECT DETAILS
  - Zebrafish and Mice
- METHOD DETAILS
  - Generation of *cyp24a1*^{mGFP} Zebrafish
  - Generation of *ubb:cyp24a1* Zebrafish
  - Generation of *hsp70:dn-vdra* and *hsp70:dn-vdrb* Zebrafish
  - Generation of *cmlc2:dn-vdra* and *cmlc2:ca-vdra* Zebrafish
  - Generation of *krtt1c19e:H2A-mCherry* Zebrafish
  - Generation of *fabp10a:dn-vdra* and *fabp10a:ca-vdra* Zebrafish
  - Generation of *vdra* and *vdrb* Mutant Zebrafish
  - Chemical Screening and Drug Treatment
  - Epicardial Explants Culture and Imaging
  - Mouse Cardiomyocyte Cultures
  - Histology and Imaging
  - RNA Sequencing and Quantitative PCR
  - Metabolomic Analysis
- QUANTIFICATION AND STATISTICAL ANALYSIS
- DATA AND SOFTWARE AVAILABILITY

SUPPLEMENTAL INFORMATION

Supplemental Information includes four figures, three tables, and one video and can be found with this article online at https://doi.org/10.1016/j.devcel.2019.01.001.

ACKNOWLEDGMENTS

We thank Duke Zebrafish Core Facilities staff for zebrafish care; Duke Computing Cluster for computing support; Duke University Proteomics and Metabolomics Core Facility for metabolomics analysis; A. Arnold for PS121912; J. Rawls and B. Link for DNA constructs; M. Bagnat, M. Goll, and D. Shin for zebrafish lines; R. Karra and N. Bursac for discussions; and J. Kang for comments on the manuscript. This work was supported by predoctoral fellowships from the American Heart Association (AHA) to A.C. and the National Science Foundation to V.A.T. and B.D.C.; postdoctoral fellowships from AHA to J.C., from the Swiss National Science Foundation to V.C., and from the National Institutes of Health (NIH) to W.-Y.C.; grants from the NIH (R01 HL081674, R01 GM074057, R01 HL136182, and R01 HL131319), the March of Dimes, and the AHA to K.D.P.; and a grant from Fondation Leducq to K.D.P. and E.T.

AUTHOR CONTRIBUTIONS

Conceptualization, Y.H., W.-Y.C., and K.D.P.; Methodology, Y.H., W.-Y.C., and K.-B.U.; Investigation, Y.H., A.C., K.-B.U., K.A.O., W.-Y.C., A.L.D., and O.Y.; Writing – Original Draft, Y.H., K.-B.U., and K.D.P.; Writing – Review & Editing, Y.H. and K.D.P.; Funding Acquisition, A.C., V.A.T., B.D.C., J.C., V.C., W.-Y.C., E.T., and K.D.P.; Resources, Y.H., A.C., K.A.O., V.C., J.C., V.A.T., and B.D.C.; Visualization, Y.H. and J.O.; Supervision, K.D.P. and E.T.

DECLARATION OF INTERESTS

The authors declare no competing interests.

Received: August 23, 2018
Revised: November 15, 2018
Accepted: December 28, 2018
Published: January 31, 2019

REFERENCES

Asakawa, K., Suster, M.L., Mizusawa, K., Nagayoshi, S., Kotani, T., Urasaki, A., Kishimoto, Y., Hibi, M., and Kawakami, K. (2008). Genetic dissection of neural circuits by Tol2 transposon-mediated Gal4 gene and enhancer trapping in zebrafish. Proc. Natl. Acad. Sci. U S A *105*, 1255–1260.

Bae, S., Singh, S.S., Yu, H., Lee, J.Y., Cho, B.R., and Kang, P.M. (1985). Vitamin D signaling pathway plays an important role in the development of heart failure after myocardial infarction. J. Appl. Physiol. *114*, 979–987.

Bassat, E., Mutlak, Y.E., Genzelinakh, A., Shadrin, I.Y., Baruch Umansky, K., Yifa, O., Kain, D., Rajchman, D., Leach, J., Riabov Bassat, D., et al. (2017). The extracellular matrix protein agrin promotes heart regeneration in mice. Nature *547*, 179–184.

Bergmann, O., Bhardwaj, R.D., Bernard, S., Zdunek, S., Barnabe-Heider, F., Walsh, S., Zupicich, J., Alkass, K., Buchholz, B.A., Druid, H., et al. (2009). Evidence for cardiomyocyte renewal in humans. Science *324*, 98–102.

Bergmann, O., Zdunek, S., Felker, A., Salehpour, M., Alkass, K., Bernard, S., Sjostrom, S.L., Szewczykowska, M., Jackowska, T., Dos Remedios, C., et al. (2015). Dynamics of cell generation and turnover in the human heart. Cell *161*, 1566–1575.

Bersell, K., Arab, S., Haring, B., and Kuhn, B. (2009). Neuregulin1/ErbB4 signaling induces cardiomyocyte proliferation and repair of heart injury. Cell *138*, 257–270.

Bikle, D.D. (2014). Vitamin D metabolism, mechanism of action, and clinical applications. Chem. Biol. *21*, 319–329.

Campbell, M.J., and Trump, D.L. (2017). Vitamin D receptor signaling and cancer. Endocrinol. Metab. Clin. North Am. *46*, 1009–1038.

Cao, J., Wang, J., Jackman, C.P., Cox, A.H., Trembley, M.A., Balowski, J.J., Cox, B.D., De Simone, A., Dickson, A.L., Di Talia, S., et al. (2017). Tension creates an endoreplication wavefront that leads regeneration of epicardial tissue. Dev. Cell *42*, 600–615.e4.

Carlberg, C., and Seuter, S. (2009). A genomic perspective on vitamin D signaling. Anticancer Res. *29*, 3485–3493.

Chen, S., Law, C.S., Grigsby, C.L., Olsen, K., Hong, T.T., Zhang, Y., Yeghiazarians, Y., and Gardner, D.G. (2011). Cardiomyocyte-specific deletion of the vitamin D receptor gene results in cardiac hypertrophy. Circulation *124*, 1838–1847.

(D) Quantification of FUCCI$^+$ CMs of 4 dpf *cmlc2:FUCCI* embryos after 24-h treatment. Mean ± SD, Mann-Whitney test and Student's t test. ns, not significant; ***$p < 0.001$. n = 11.
(E) MIP images of dissected 4 dpf hearts after 24-h treatment. Scale bar, 50 μm.
(F) Quantification of FUCCI$^+$ CMs of 4 dpf embryos after 24-h treatment. Mean ± SD, Mann-Whitney test and Student's t test. **$p < 0.01$; ****$p < 0.0001$. n = 8–11.
(G) PCNA/Mef2 staining of ventricles from Alfa-injected zebrafish treated with vehicle or AG1478 for 24 h, starting at 2 h after the last Alfa injection. Scale bar, 100 μm.
(H) Quantification of CM proliferation indices of experiments in (H). Mean ± SD, Student's t test. n = 9.
See also Figure S4; Tables S2 and S3.

Choi, T.Y., Ninov, N., Stainier, D.Y., and Shin, D. (2014). Extensive conversion of hepatic biliary epithelial cells to hepatocytes after near total loss of hepatocytes in zebrafish. Gastroenterology *146*, 776–788.

Choi, W.Y., Gemberling, M., Wang, J., Holdway, J.E., Shen, M.C., Karlstrom, R.O., and Poss, K.D. (2013). *In vivo* monitoring of cardiomyocyte proliferation to identify chemical modifiers of heart regeneration. Development *140*, 660–666.

Choudhury, S., Bae, S., Ke, Q., Lee, J.Y., Singh, S.S., St-Arnaud, R., Monte, F.D., and Kang, P.M. (2014). Abnormal calcium handling and exaggerated cardiac dysfunction in mice with defective vitamin d signaling. PLoS One *9*, e108382.

Cortes, M., Chen, M.J., Stachura, D.L., Liu, S.Y., Kwan, W., Wright, F., Vo, L.T., Theodore, L.N., Esain, V., Frost, I.M., et al. (2016). Developmental vitamin D availability impacts hematopoietic stem cell production. Cell Rep. *17*, 458–468.

Cox, B.D., De Simone, A., Tornini, V.A., Singh, S.P., Di Talia, S., and Poss, K.D. (2018). In toto imaging of dynamic osteoblast behaviors in regenerating skeletal bone. Curr. Biol. *28*, 3937–3947.e4.

D'Uva, G., Aharonov, A., Lauriola, M., Kain, D., Yahalom-Ronen, Y., Carvalho, S., Weisinger, K., Bassat, E., Rajchman, D., Yifa, O., et al. (2015). ERBB2 triggers mammalian heart regeneration by promoting cardiomyocyte dedifferentiation and proliferation. Nat. Cell Biol. *17*, 627–638.

Dang, R., Guo, Y., Zhu, Y., Yang, R., Cai, H., and Jiang, P. (2016). Chronic administration of calcitriol enhanced neuregulin-1/ErbB signaling in rat myocardium. Pharmazie *71*, 192–195.

Engler, C., Kandzia, R., and Marillonnet, S. (2008). A one pot, one step, precision cloning method with high throughput capability. PLoS One *3*, e3647.

Foglia, M.J., Cao, J., Tornini, V.A., and Poss, K.D. (2016). Multicolor mapping of the cardiomyocyte proliferation dynamics that construct the atrium. Development *143*, 1688–1696.

Ford, K., Latic, N., Slavic, S., Zeitz, U., Dolezal, M., Andrukhov, O., Erben, R.G., and Andrukhova, O. (2018). Lack of vitamin D signalling per se does not aggravate cardiac functional impairment induced by myocardial infarction in mice. PLoS One *13*, e0204803.

Gemberling, M., Karra, R., Dickson, A.L., and Poss, K.D. (2015). Nrg1 is an injury-induced cardiomyocyte mitogen for the endogenous heart regeneration program in zebrafish. Elife *4*, https://doi.org/10.7554/eLife.05871.

Gonzalez-Rosa, J.M., Sharpe, M., Field, D., Soonpaa, M.H., Field, L.J., Burns, C.E., and Burns, C.G. (2018). Myocardial polyploidization creates a barrier to heart regeneration in zebrafish. Dev. Cell *44*, 433–446.e7.

Han, Y., Mu, Y., Li, X., Xu, P., Tong, J., Liu, Z., Ma, T., Zeng, G., Yang, S., Du, J., et al. (2011). Grhl2 deficiency impairs otic development and hearing ability in a zebrafish model of the progressive dominant hearing loss DFNA28. Hum. Mol. Genet. *20*, 3213–3226.

Hassink, R.J., Pasumarthi, K.B., Nakajima, H., Rubart, M., Soonpaa, M.H., de la Riviere, A.B., Doevendans, P.A., and Field, L.J. (2008). Cardiomyocyte cell cycle activation improves cardiac function after myocardial infarction. Cardiovasc. Res. *78*, 18–25.

Heallen, T., Morikawa, Y., Leach, J., Tao, G., Willerson, J.T., Johnson, R.L., and Martin, J.F. (2013). Hippo signaling impedes adult heart regeneration. Development *140*, 4683–4690.

Hlaing, S.M., Garcia, L.A., Contreras, J.R., Norris, K.C., Ferrini, M.G., and Artaza, J.N. (2014). 1,25-Vitamin D3 promotes cardiac differentiation through modulation of the WNT signaling pathway. J. Mol. Endocrinol. *53*, 303–317.

Huang, C.J., Tu, C.T., Hsiao, C.D., Hsieh, F.J., and Tsai, H.J. (2003). Germ-line transmission of a myocardium-specific GFP transgene reveals critical regulatory elements in the cardiac myosin light chain 2 promoter of zebrafish. Dev. Dyn. *228*, 30–40.

Huang da, W., Sherman, B.T., and Lempicki, R.A. (2009). Bioinformatics enrichment tools: paths toward the comprehensive functional analysis of large gene lists. Nucleic Acids Res. *37*, 1–13.

Jopling, C., Sleep, E., Raya, M., Marti, M., Raya, A., and Izpisua Belmonte, J.C. (2010). Zebrafish heart regeneration occurs by cardiomyocyte dedifferentiation and proliferation. Nature *464*, 606–609.

Kikuchi, K., Holdway, J.E., Major, R.J., Blum, N., Dahn, R.D., Begemann, G., and Poss, K.D. (2011). Retinoic acid production by endocardium and epicardium is an injury response essential for zebrafish heart regeneration. Dev. Cell *20*, 397–404.

Kikuchi, K., Holdway, J.E., Werdich, A.A., Anderson, R.M., Fang, Y., Egnaczyk, G.F., Evans, T., Macrae, C.A., Stainier, D.Y., and Poss, K.D. (2010). Primary contribution to zebrafish heart regeneration by gata4(+) cardiomyocytes. Nature *464*, 601–605.

Kim, D., Pertea, G., Trapnell, C., Pimentel, H., Kelley, R., and Salzberg, S.L. (2013). TopHat2: accurate alignment of transcriptomes in the presence of insertions, deletions and gene fusions. Genome Biol. *14*, R36.

Kochhan, E., Lenard, A., Ellertsdottir, E., Herwig, L., Affolter, M., Belting, H.G., and Siekmann, A.F. (2013). Blood flow changes coincide with cellular rearrangements during blood vessel pruning in zebrafish embryos. PLoS One *8*, e75060.

Kramer, A., Green, J., Pollard, J., Jr., and Tugendreich, S. (2014). Causal analysis approaches in Ingenuity Pathway Analysis. Bioinformatics *30*, 523–530.

Kwon, H.J. (2016). Vitamin D receptor signaling is required for heart development in zebrafish embryo. Biochem. Biophys. Res. Commun. *470*, 575–578.

Lee, R.T., Asharani, P.V., and Carney, T.J. (2014). Basal keratinocytes contribute to all strata of the adult zebrafish epidermis. PLoS One *9*, e84858.

Lee, Y., Grill, S., Sanchez, A., Murphy-Ryan, M., and Poss, K.D. (2005). .Fgf signaling instructs position-dependent growth rate during zebrafish fin regeneration. Development *132*, 5173–5183.

Liao, Y., Smyth, G.K., and Shi, W. (2014). featureCounts: an efficient general purpose program for assigning sequence reads to genomic features. Bioinformatics *30*, 923–930.

Lin, C.H., Su, C.H., Tseng, D.Y., Ding, F.C., and Hwang, P.P. (2012). Action of vitamin D and the receptor, VDRa, in calcium handling in zebrafish (Danio rerio). PLoS One *7*, e45650.

Ma, Y., Johnson, C.S., and Trump, D.L. (2016). Mechanistic insights of vitamin D anticancer effects. Vitam. Horm. *100*, 395–431.

Malloy, P.J., Zhou, Y., Wang, J., Hiort, O., and Feldman, D. (2011). Hereditary vitamin D-resistant rickets (HVDRR) owing to a heterozygous mutation in the vitamin D receptor. J. Bone Miner. Res. *26*, 2710–2718.

Merrigan, S.L., and Kennedy, B.N. (2017). Vitamin D receptor agonists regulate ocular developmental angiogenesis and modulate expression of dre-miR-21 and VEGF. Br. J. Pharmacol. *174*, 2636–2651.

Mohamed, T.M.A., Ang, Y.S., Radzinsky, E., Zhou, P., Huang, Y., Elfenbein, A., Foley, A., Magnitsky, S., and Srivastava, D. (2018). Regulation of cell cycle to stimulate adult cardiomyocyte proliferation and cardiac regeneration. Cell *173*, 104–116.e12.

Montague, T.G., Cruz, J.M., Gagnon, J.A., Church, G.M., and Valen, E. (2014). CHOPCHOP: a CRISPR/Cas9 and TALEN web tool for genome editing. Nucleic Acids Res. *42*, W401–W407.

Mosimann, C., Kaufman, C.K., Li, P., Pugach, E.K., Tamplin, O.J., and Zon, L.I. (2011). Ubiquitous transgene expression and Cre-based recombination driven by the ubiquitin promoter in zebrafish. Development *138*, 169–177.

Nibbelink, K.A., Tishkoff, D.X., Hershey, S.D., Rahman, A., and Simpson, R.U. (2007). 1,25(OH)2-vitamin D3 actions on cell proliferation, size, gene expression, and receptor localization, in the HL-1 cardiac myocyte. J. Steroid Biochem. Mol. Biol. *103*, 533–537.

Ninov, N., Borius, M., and Stainier, D.Y. (2012). Different levels of Notch signaling regulate quiescence, renewal and differentiation in pancreatic endocrine progenitors. Development *139*, 1557–1567.

O'Connell, T.D., Berry, J.E., Jarvis, A.K., Somerman, M.J., and Simpson, R.U. (1997). 1,25-dihydroxyvitamin D3 regulation of cardiac myocyte proliferation and hypertrophy. Am. J. Physiol. *272*, H1751–H1758.

Patterson, M., Barske, L., Van Handel, B., Rau, C.D., Gan, P., Sharma, A., Parikh, S., Denholtz, M., Huang, Y., Yamaguchi, Y., et al. (2017). Frequency of mononuclear diploid cardiomyocytes underlies natural variation in heart regeneration. Nat. Genet. *49*, 1346–1353.

Peng, X., Shang, G., Wang, W., Chen, X., Lou, Q., Zhai, G., Li, D., Du, Z., Ye, Y., Jin, X., et al. (2017). Fatty acid oxidation in zebrafish adipose tissue is promoted by 1alpha,25(OH)2D3. Cell Rep. *19*, 1444–1455.

Pilz, S., Verheyen, N., Grubler, M.R., Tomaschitz, A., and Marz, W. (2016). Vitamin D and cardiovascular disease prevention. Nat. Rev. Cardiol. *13*, 404–417.

Porrello, E.R., Mahmoud, A.I., Simpson, E., Hill, J.A., Richardson, J.A., Olson, E.N., and Sadek, H.A. (2011). Transient regenerative potential of the neonatal mouse heart. Science *331*, 1078–1080.

Poss, K.D., Wilson, L.G., and Keating, M.T. (2002). Heart regeneration in zebrafish. Science *298*, 2188–2190.

Ringe, J.D., and Schacht, E. (2007). Improving the outcome of established therapies for osteoporosis by adding the active D-hormone analog alfacalcidol. Rheumatol. Int. *28*, 103–111.

Robinson, M.D., McCarthy, D.J., and Smyth, G.K. (2010). edgeR: a bioconductor package for differential expression analysis of digital gene expression data. Bioinformatics *26*, 139–140.

Sakaue-Sawano, A., Kurokawa, H., Morimura, T., Hanyu, A., Hama, H., Osawa, H., Kashiwagi, S., Fukami, K., Miyata, T., Miyoshi, H., et al. (2008). Visualizing spatiotemporal dynamics of multicellular cell-cycle progression. Cell *132*, 487–498.

Salic, A., and Mitchison, T.J. (2008). A chemical method for fast and sensitive detection of DNA synthesis *in vivo*. Proc. Natl. Acad. Sci. U S A *105*, 2415–2420.

Samuel, S., and Sitrin, M.D. (2008). Vitamin D's role in cell proliferation and differentiation. Nutr. Rev. *66*, S116–S124.

Sidhu, P.S., Nassif, N., McCallum, M.M., Teske, K., Feleke, B., Yuan, N.Y., Nandhikonda, P., Cook, J.M., Singh, R.K., Bikle, D.D., et al. (2014). Development of novel vitamin D receptor-coactivator inhibitors. ACS Med. Chem. Lett. *5*, 199–204.

Simpson, R.U., Hershey, S.H., and Nibbelink, K.A. (2007). Characterization of heart size and blood pressure in the vitamin D receptor knockout mouse. J. Steroid Biochem. Mol. Biol. *103*, 521–524.

Tebben, P.J., Singh, R.J., and Kumar, R. (2016). Vitamin D-mediated hypercalcemia: mechanisms, diagnosis, and treatment. Endocr. Rev. *37*, 521–547.

Varshney, G.K., Pei, W., LaFave, M.C., Idol, J., Xu, L., Gallardo, V., Carrington, B., Bishop, K., Jones, M., Li, M., et al. (2015). High-throughput gene targeting and phenotyping in zebrafish using CRISPR/Cas9. Genome Res. *25*, 1030–1042.

von Gise, A., Lin, Z., Schlegelmilch, K., Honor, L.B., Pan, G.M., Buck, J.N., Ma, Q., Ishiwata, T., Zhou, B., Camargo, F.D., et al. (2012). YAP1, the nuclear target of Hippo signaling, stimulates heart growth through cardiomyocyte proliferation but not hypertrophy. Proc. Natl. Acad. Sci. U S A *109*, 2394–2399.

Wang, J., Panakova, D., Kikuchi, K., Holdway, J.E., Gemberling, M., Burris, J.S., Singh, S.P., Dickson, A.L., Lin, Y.F., Sabeh, M.K., et al. (2011). The regenerative capacity of zebrafish reverses cardiac failure caused by genetic cardiomyocyte depletion. Development *138*, 3421–3430.

Wills, A.A., Holdway, J.E., Major, R.J., and Poss, K.D. (2008). Regulated addition of new myocardial and epicardial cells fosters homeostatic cardiac growth and maintenance in adult zebrafish. Development *135*, 183–192.

Xin, M., Kim, Y., Sutherland, L.B., Murakami, M., Qi, X., McAnally, J., Porrello, E.R., Mahmoud, A.I., Tan, W., Shelton, J.M., et al. (2013). Hippo pathway effector Yap promotes cardiac regeneration. Proc. Natl. Acad. Sci. U S A *110*, 13839–13844.

Yao, T., Ying, X., Zhao, Y., Yuan, A., He, Q., Tong, H., Ding, S., Liu, J., Peng, X., Gao, E., et al. (2015). Vitamin D receptor activation protects against myocardial reperfusion injury through inhibition of apoptosis and modulation of autophagy. Antioxid. Redox Signal. *22*, 633–650.

Ye, L., D'Agostino, G., Loo, S.J., Wang, C.X., Su, L.P., Tan, S.H., Tee, G.Z., Pua, C.J., Pena, E.M., Cheng, R.B., et al. (2018). Early regenerative capacity in the porcine heart. Circulation *138*, 2798–2808.

Zhu, W., Zhang, E., Zhao, M., Chong, Z., Fan, C., Tang, Y., Hunter, J.D., Borovjagin, A.V., Walcott, G.P., Chen, J.Y., et al. (2018). Regenerative potential of neonatal porcine hearts. Circulation *138*, 2809–2816.

STAR★METHODS

KEY RESOURCES TABLE

REAGENT or RESOURCE	SOURCE	IDENTIFIER
Antibodies		
Rabbit polyclonal anti-phospho-Histone H3 (Ser10)	Cell Signaling Technology	Cat#9701; RRID:AB_331535
Mouse polyclonal anti-phospho-Histone H3 (Ser10)	Cell Signaling Technology	Cat#9706; RRID:AB_331748
Rabbit polyclonal anti-Mef-2	Santa Cruz Biotechnology	Cat#sc-313; RRID:AB_631920
Mouse monoclonal anti-PCNA	Sigma-Aldrich	Cat#P8825; RRID:AB_477413
Rabbit monoclonal anti-HNF-4-alpha	Abcam	Cat#ab201460
Mouse monoclonal anti-Troponin T	Lab Vision	Cat#MS-295-PABX; RRID:AB_61810
Mouse monoclonal anti-cardiac Troponin T	Abcam	Cat#ab33589; RRID:AB_727035
Mouse monoclonal anti-Ki-67	Cell Marque Corp	Cat#275R; RRID:AB_1158031
Rat monoclonal anti-Ki-67, eFlour 570 conjugated	Thermo Fisher Scientific	Cat#41-5698-80; RRID:AB_11219874
Mouse monoclonal anti-p63	Biocare Medical	Cat#CM163A; RRID:AB_10582730
Alexa Fluor 488 Goat anti-Rabbit IgG (H+L)	Thermo Fisher Scientific	Cat#A-11034; RRID:AB_2576217
Alexa Fluor 488 Goat anti-Mouse IgG (H+L)	Thermo Fisher Scientific	Cat#A-11001; RRID:AB_2534069
Alexa Fluor 546 Goat anti-Rabbit IgG (H+L)	Thermo Fisher Scientific	Cat#A-11035; RRID:AB_143051
Alexa Fluor 546 Goat anti-Mouse IgG (H+L)	Thermo Fisher Scientific	Cat#A-11030; RRID:AB_144695
Alexa Fluor 594 Goat anti-Rabbit IgG (H+L)	Thermo Fisher Scientific	Cat#A-11037; RRID:AB_2534095
Alexa Fluor 594 Goat anti-Mouse IgG (H+L)	Thermo Fisher Scientific	Cat#A-11032; RRID:AB_141672
Chemicals, Peptides, and Recombinant Proteins		
Metronidazole	Sigma-Aldrich	Cat#M1547
Fibronectin	Thermo Fisher Scientific	Cat#33010018
5-ethynyl-2′-deoxyuridine	Thermo Fisher Scientific	Cat#A10044
AG-1478	Selleck Chemicals	Cat#S2728
Alfacalcidol	Selleck Chemicals	Cat#S1468
Calcitriol	Selleck Chemicals	Cat#S1466
DAPI	Thermo Fisher Scientific	Cat#D3571
Alexa Fluor 488 Azide	Thermo Fisher Scientific	Cat#A10266
Alexa Fluor 594 Azide	Thermo Fisher Scientific	Cat#A10270
Alexa Fluor 488 Click-iT Plus TUNEL Assay	Thermo Fisher Scientific	Cat#C10617
Prestwick Chemical Library	Prestwick Chemical	N/A
PS121912	University of Wisconsin-Milwaukee	N/A
Deposited Data		
RNA Sequencing	GEO database	GSE112826

(*Continued on next page*)

Continued

REAGENT or RESOURCE	SOURCE	IDENTIFIER
Experimental Models: Organisms/Strains		
Zebrafish: *Tg(cmlc2:mCherry-zCdt1)^{pd57}*	Choi et al., 2013	*pd57*
Zebrafish: *Tg(cmlc2:Venus-hGeminin)^{pd58}*	Choi et al., 2013	*pd58*
Zebrafish: *Tg(cmlc2:H2A-EGFP)^{pd115}*	Foglia et al., 2016	*pd115*
Zebrafish: *Tg(tcf21:mAG-zGeminin)^{pd254}*	Cao et al., 2017	*pd254*
Zebrafish: *Tg(tcf21:zCdt1-mKO2)^{pd255}*	Cao et al., 2017	*pd255*
Zebrafish: *Tg(kdrl:H2B-EGFP)^{mu122}*	Kochhan et al., 2013	*mu122*
Zebrafish: Tg(bactin2:loxP-mCherry-STOP-loxP-DTA176)^{pd36}	Wang et al., 2011	*pd36*
Zebrafish: *Tg(Tp1:H2B-mCherry)*	Ninov et al., 2012	N/A
Zebrafish: *Tg(fabp10a:nls-mCherry)*	Choi et al., 2014	N/A
Zebrafish: *Tg(krtt1c19e:H2A-mCherry)^{pd309}*	This paper	*pd309*
Zebrafish: *Tg(osx:mCherry-zCdt1)^{pd270}*	Cox et al., 2018	*pd270*
Zebrafish: *Tg(osx:Venus-hGeminin)^{pd271}*	Cox et al., 2018	*pd271*
Zebrafish: *cyp24a1^{mGFP}*	This paper	*pd272*
Zebrafish: *Tg(ubb:cyp24a1) ^{pd273}*	This paper	*pd273*
Zebrafish: *Tg(ubb:cyp24a1)^{pd274}*	This paper	*pd274*
Zebrafish: *Tg(hsp70:dn-vdra)^{pd276}*	This paper	*pd276*
Zebrafish: *Tg(cmlc2:dn-vdra)^{pd301}*	This paper	*pd301*
Zebrafish: *Tg(cmlc2:ca-vdra)^{pd302}*	This paper	*pd302*
Zebrafish: *Tg(fabp10a:dn-vdra)^{pd303}*	This paper	*pd303*
Zebrafish: *Tg(fabp10a:ca-vdra)^{pd304}*	This paper	*pd304*
Zebrafish: *vdra^{pd307}*	This paper	*pd307*
Zebrafish: *vdrb^{pd308}*	This paper	*pd308*
Software and Algorithms		
Tophat2	Kim et al., 2013	Version 2.1.1
featureCounts	Liao et al., 2014	Version 1.5.3
edgeR	Robinson et al., 2010	Version 3.20.9
DAVID Bioinformatics Resources	Huang da et al., 2009	Version 6.8
Ingenuity Pathway Analysis	Qiagen, Kramer et al., 2014	830011

CONTACT FOR REAGENT AND RESOURCE SHARING

Further information and requests for resources and reagents should be directed to and will be fulfilled by the Lead Contact, Kenneth Poss (kenneth.poss@duke.edu).

EXPERIMENTAL MODEL AND SUBJECT DETAILS

Zebrafish and Mice

Wild-type or transgenic male and female zebrafish of the outbred Ekkwill and Ekkwill/AB strains were used in this study. Four to 12-month-old zebrafish were used for adult experiments, and ages of embryonic and juvenile zebrafish were indicated in the text. Water temperature was maintained at 28°C for embryos up to 5 dpf and 27°C afterwards. After transfer to system racks at 5 dpf, all fish were fed with artemia and age-dependent dry diets, i.e., Larval AP100 Z1 to Z3 (Zeigler) for 5–14 dpf, GEMMA Micro 75 for 2–4 wpf, GEMMA Micro 150 for 4–5 wpf, GEMMA Micro 300 for 5 wpf to 3 mpf and a mixture of GEMMA Micro 500 and Gemma Wean Diamond 0.5 after 3 mpf. The vitamin D3 levels in the diet are 2800 IU/kg for GEMMA Micro and 2400 IU/kg for Gemma Wean Diamond. All transgenic strains were analyzed as hemizygotes unless otherwise indicated. Partial ventricular resection surgeries were performed as previously described (Poss et al., 2002). Briefly, animals were anaesthetized and placed ventral side up in a prepared sponge bed. Straight iridectomy scissors were used to make a small incision through the ventral body and pericardial sac, and curved iridectomy scissors were used to remove approximately 20% of the cardiac ventricle. To genetically ablate ~50% of cardiomyocytes, zebrafish with *cmlc2:CreER^{pd10}; bactin2:loxp-mCherry-STOP-loxp-DTA^{pd36}* transgenes were treated with 0.5 μM tamoxifen for 16 h and hearts were collected 7 days later (Wang et al., 2011). For embryonic heat shock experiments, animals maintained at 28°C were incubated at 38°C for 30 minutes and then washed with egg water at room temperature. For adult heat

shock experiments, animals maintained at 28°C were heat shocked daily at 37 to 38°C for 30 minutes as described (Lee et al., 2005), starting at 6 days post-surgery until tissues were harvested. All zebrafish procedures were performed in accordance with animal use guidelines at Duke University. Neonatal day 7 (P7) P7 ICR mice were used to isolate and culture primary cardiac cells. Animal procedures were approved by Animal Care and Use Committees of Duke University and the Weizmann Institute of Science.

METHOD DETAILS

Generation of *cyp24a1*^{mGFP} Zebrafish

To insert an mGFP-polyA cassette into the *cyp24a1* locus, we designed a TALEN pair (left arm: 5'-GACAACTTTTACGCACG-3', right arm: 5'-GCGCTCTCATCTTGAG-3') targeting the start codon region of *cyp24a1* gene. After validating the efficiency of the TALEN nuclease, we introduced the TALEN sequences and a common right arm sequence (5'-GTATACTACTGCGGCTAT-3') into a donor vector that contains a *mGFP-polyA* reporter cassette, a ubiquitous *ef1α:mCherry-polyA* reporter cassette, and two FRT sequences flanking the vector sequences (Figure S1B). Then, the three TALEN nuclease mRNAs and donor vector were co-injected into one-cell stage embryos. The vector-free stable mGFP^{+}mCherry^{-} transgenic embryos were screened under a stereofluorescence microscope and further confirmed by PCR and Sanger sequencing.

Generation of *ubb:cyp24a1* Zebrafish

The full-length *cyp24a1* coding sequences were amplified from 2 dpf zebrafish cDNA using the following primers: forward 5'-GAA TTT GTT TAC AGG GAT CCA CCG GTG CCA CCA TGA GAG CGC ACT TGC A-3' and reverse 5'-GAA GTT TGT AGC GCC GCT TCC GGA GCG TGG AAC AAA AGC CA-3'. 3.8 kb *ubb* promoter sequences (Mosimann et al., 2011) were amplified from adult genomic DNA using the following primers: forward 5'-CCA CCT CGA GGC TGT GAC ATG GTG TT-3' and reverse 5'-GAC TAC CGG TGG ATC CCT GTA AAC AAA TTC AAA GTA AGA TTA GC-3'. Then, the two sequences were subcloned sequentially into a P2A-TagBFP vector. Purified plasmid was linearized with I-SceI meganuclease and injected into one-cell stage embryos. Stable transgenic embryos were screened under a stereofluorescence microscope.

Generation of *hsp70:dn-vdra* and *hsp70:dn-vdrb* Zebrafish

Full-length coding sequences of *vdra* were amplified from zebrafish embryonic cDNA and subcloned into an mRNA *in vitro* transcription vector using the following primers: *vdra*-forward, 5'-CTC GAA TTC ACC GGT CAC CAT GCT TAC GGA AAA TAG TGC C-3'; *vdra*-reverse, 5'-GGT ACT AGT CGG CCG CTA GGA CAC CTC ACT CC-3'. Human E420A-equivalent dominant negative mutations (Malloy et al., 2011) were introduced using the following primers: *vdra*-mut, 5'-CGC ACT AGT CGG CCG CTA GGA CAC CTC ACT CCC GAA CAC AGC CAG CACCAG-3'. Wild-type and dominant-negative *vdr* gene cassettes were transcribed, and mRNA was injected into one-cell stage *cyp24a1*^{mGFP} embryos to test their effects on *cyp24a1* expression. The *hsp70* promoter was PCR amplified from an *hsp70* vector (Han et al., 2011) using the following primers: *hsp70*-forward, 5'-CTT CGT CTC AGT ACC CTC GAG TCA GGG GTG TCG CTT GGT T-3'; *hsp70*-reverse, 5'-GCT CGT CTC AGG ATC CGA TTG ATT TCA AGA AAC TGC AA-3'. Then, the *hsp70* promoter fragment and in-frame *dn-vdra* sequences were amplified and subcloned into the P2A-TagBFP vector. Stable transgenic lines were generated using I-SceI-mediated transgenesis and screened under a stereofluorescence microscope following heat shock.

Generation of *cmlc2:dn-vdra* and *cmlc2:ca-vdra* Zebrafish

E420A-equivalent *dn-vdra* sequences were excised from the *hsp70:dn-vdra* construct and subcloned into a 5 kb *cmlc2* promoter construct using AgeI and NotI. Stable transgenic lines were generated using I-SceI-mediated transgenesis and screened under a stereofluorescence microscope. To generate the constitutively active *vdra* construct, the FF version of dual-VP16 sequences (Asakawa et al., 2008) was synthesized from Integrated DNA Technologies and fused to 3' end of wild-type *vdra* sequences, referred to as *ca-vdra*. Then, a 900 bp *cmlc2* promoter fragment (Huang et al., 2003) and *ca-vdra-P2A-TagBFP2* sequences were subcloned into a *Tol2*/I-SceI construct using Golden Gate cloning (Engler et al., 2008). Stable transgenic lines were generated using *Tol2*-mediated transgenesis and screened under a stereofluorescence microscope.

Generation of *krtt1c19e:H2A-mCherry* Zebrafish

The 4 kb *krtt1c19e* promoter sequence (Lee et al., 2014) was amplified using the primers 5'-CCG CGG CAA CAA CAA TCC ACC TCA AGA GT-3' to add a SacII site to the 5' end and 5'-GGA TCC GAT GGT GGT TGG TGT CTT ACT CTG-3' to add a BamHI site to the 3' end, then digested with those restriction enzymes and subcloned into the pSKS-1 vector. H2A-mCherry-polyA sequence was amplified using primers 5'-ATC GAT GCC GCC ACC ATG GCA GGT GGA AAA GCA GG-3' to add a ClaI site to the 5' end and 5'-CTC GAG GAT ACA TTG ATG AGT TTG GAC AAA CC-3' to add a XhoI site the the 3' end, then subcloned into the *krtt1c19e* promoter-containing vector. The resulting plasmid was purified and injected into one-cell stage embryos.

Generation of *fabp10a:dn-vdra* and *fabp10a:ca-vdra* Zebrafish

dn-vdra-2A-TagBFP2 and *ca-vdra-2A-TagBFP2* sequences were subcloned into middle entry vectors and subjected to Gateway cloning with a p5E-*fabp10a* entry vector (a kind gift from Drs. Brian Link and John Rawls) and a *Tol2*/I-SceI destination vector to generate final *fabp10a:dn-vdra* and *fabp10a:ca-vdra* vectors. Stable transgenic lines were generated using *Tol2*-mediated transgenesis and screened under a stereofluorescence microscope.

Generation of *vdra* and *vdrb* Mutant Zebrafish

vdra and *vdrb* knockout alleles were generated using CRISPR/Cas9 techniques. Two guide RNAs targeting sequences encoding DNA binding domains of Vdra and Vdrb proteins were designed using CHOPCHOP website (Montague et al., 2014), synthesized as described (Varshney et al., 2015) and co-injected with Cas9 protein (PNA Bio) to generate deletional *vdra* and *vdrb* mutants lacking functional DNA binding domain. Target sequences of guide RNAs are 5'-GGCGTTGAAGTGGAATCCGGTGG-3' and 5'- GATCAT CAACTCTCTGGTGGAGG-3' for *vdra*, 5'-GAACTCATCTGGCACTTGAGTGG-3' and 5'-GAAGCGTGAAAAGTCAGAGTAGG-3' for *vdrb* (underlined trinucleotides indicate PAM sequences). Injected embryos were raised to adulthood and screened as sperm samples and/or F_1 embryos using the following primers: *vdra*-fwd: 5'-TCTCTCAGCCAATCAGGAGTG-3', *vdra*-rev: 5'-TAATAGATCA GAGCAGCCGAC-3'; *vdrb*-fwd: 5'-CTTCAGGTAAACGTGCACACA-3', *vdrb*-rev: 5'-TACCGGCAGAGAAAAGGTCAT-3'.

Chemical Screening and Drug Treatment

cmlc2:FUCCI zebrafish were crossed with wild-type AB strain animals to produce hemizygous embryos. Five 3 dpf embryos were placed into each well of 48-well plates containing 0.5 mL fish water for initial screening using Prestwick Chemical Library (http://www.prestwickchemical.com/libraries-screening-lib-pcl.html). Then, embryos were treated with 5 μM compounds for 24 hours before examination using a stereofluorescence microscope. Embryos visually scored with more or fewer Venus-positive CMs were fixed with 4% paraformaldehyde (PFA) and analyzed by confocal microscopy.

For vitamin D agonist or antagonist treatment, alfacalcidol (S1468, Selleck Chemicals) and calcitriol (S1466, Selleck Chemicals) were dissolved in DMSO (for embryos) or ethanol (for injection into adults) to make 10 mM stock solutions. Final concentrations were 5 μM and 1 μM, respectively, unless otherwise indicated for embryo treatment. For adult injections, drugs were diluted with ethanol and water to make 200 μM injection-ready solutions in 10% ethanol. Then, 3 daily 10 μL solution were injected intraperitoneally into adult zebrafish unless otherwise indicated. For long-term treatment and rescue experiments, juvenile zebrafish were incubated in aquarium water with Vehicle or 10 nM alfacalcidol and fed with artemia twice every day. Fish water was changed every other day to maintain quality. PS121912 was a kind gift from Dr. Alexander Arnold (Sidhu et al., 2014). AG-1478 (S2728, Selleck Chemicals) were purchased and dissolved in DMSO to make 10 mM stock solutions.

Epicardial Explants Culture and Imaging

tcf21:FUCCI hearts were collected, cut into large pieces, and cultured using Fibronectin-coated dishes as described (Cao et al., 2017). Culture media were replaced with fresh media 3 days after culture and drugs were added 1–2 hours before live imaging the next day. Confocal images were captured once every 5 minutes for 3 days using a Zeiss 710 inverted microscope.

Mouse Cardiomyocyte Cultures

Primary cardiac cells were isolated as described (Bassat et al., 2017). Hearts were harvested from neonatal day 7 (P7) ICR mice, and cardiac cells were isolated using a neonatal dissociation kit (gentleMACS, Miltenyi Biotec) according to the manufacturer's instructions. Cardiac cells were cultured in gelatin-coated (0.02%, G1393, Sigma-Aldrich) 96 wells plates, using "rich" media (DMEM/F12 medium supplemented with l-glutamine, Na-pyruvate, non-essential amino acids, penicillin/streptomycin, 5% horse serum and 10% fetal bovine serum (FBS)) at 37°C and 5% CO_2, allowing them to adhere. 2 days post seeding, the medium was replaced with serum-free medium containing vehicle or 0.1 μM, 1 μM or 10 μM calcitriol for 72 hours. Cells were then fixed in 4% PFA and stained for cardiomyocyte marker (cTnT) and proliferation marker (Ki67).

Histology and Imaging

Tissues were fixed with 4% PFA, and 10 μm cryosections were used in this study. Immunofluorescence was performed as described previously (Kikuchi et al., 2011). Briefly, slides were washed in PBT (Phosphate-buffered saline + 0.1% Tween-20), blocked in NCS-PBT (PBT with 10% heat-inactivated calf serum and 1% DMSO) and 2% horse serum, and then incubated in NCS-PBT with primary antibodies at 37°C for 3 h or 4°C overnight. After washes in PBT, slides were incubated with fluorescently labeled secondary antibodies at 37°C for one hour, washed in PBT, and mounted. Staining with anti-PCNA antibodies required citrate buffer (10 mM citric acid, 0.05% Tween-20, pH 6.0) treatment, involving heating to 98°C, boiling for 25 min, and cooling for 20 min before PBT washes and blocking. For EdU incorporation, zebrafish were injected intraperitoneally with 10 μL of 10 mM EdU (A10055, Sigma) 6 hours (for fin epithelial cells) or 24 hours (for other tissues) before tissue collection. EdU was detected through a click reaction as described previously using fluorescent azide (Alexa Fluor 488 or 594, Thermo Fisher) (Salic and Mitchison, 2008). Primary antibodies used in this study were: anti-Mef2 (sc-313, Santa Cruz Biotechnology), anti-PCNA (P8825, Sigma), anti-phospho-Histone H3 (9701S, 9706S, Cell Signaling Technology), anti-Hnf4a (ab201460, Abcam), anti-p63 (CM163A, Biocare Medical), anti-cTnT (MS-295-PABX, Thermo Fisher Scientific; ab33589, Abcam), anti-Ki67 (275R, Cell Marque), anti-Ki-67 (41-5698-80, Thermo Fisher Scientific). Secondary antibodies (Invitrogen, 1:200–1:500) used in this study were highly cross-absorbed Alexa Fluor 488/546/594 goat anti-rabbit or anti-mouse antibodies. All confocal images were acquired with Zeiss LSM 700 or Zeiss LSM 880 microscopes unless otherwise stated. Acid fuchsin orange g (AFOG) stains to visualize fibrin and collagen was performed and imaged as described (Poss et al., 2002). Briefly, sections were hydrated, placed in Bouin's solution at 60°C, rinsed in water followed by 5 minutes in 1% phosphomolbdic acid and water again, then stained in an AFOG solution of 1 g analine blue, 2 g orange g, and 3 g acid fuchsin in 200 ml water, pH 1.09 for 5 minutes. Slides were then rinsed in water,

dehydrated, cleared and mounted, and imaged using a Leica DM6000 microscope. Whole-mounted tissues and embryos were imaged with a Zeiss Axio Zoom microscope.

RNA Sequencing and Quantitative PCR

Adult zebrafish were injected with vehicle or Alfa every 24 hours over 3 days, and euthanized with tricaine for heart collection 24 hours after the last injection. Total RNA from 10 pooled hearts of two biological replicates were extracted using TRIzol reagent (Invitrogen) following the manufacturer's instruction. Total RNA were treated with DNaseI to remove genomic DNA, purified with Quick-RNA MiniPrep kit (Zymo Research), and then submitted for library preparation and sequences using an Illumina HiSeq2000 at the Duke Center for Genomic and Computational Biology. Reads were mapped to the zebrafish genome (GRCz10) using Tophat2 (Kim et al., 2013), counted with featureCounts (Liao et al., 2014), and differentially expressed genes were analyzed using edgeR (Robinson et al., 2010). Functional clustering analysis was performed using the DAVID Bioinformatics Resources website (Huang da et al., 2009). The zebrafish gene IDs were mapped to human homologous gene IDs to perform pathway and upstream regulator analysis using QIAGEN Ingenuity Pathway Analysis software (Kramer et al., 2014). For qPCR, purified total RNAs were reverse transcribed with SuperScript III Reverse Transcriptase (Thermo Scientific) and qPCRs were performed using the Roche Light Cycler 480, Roche UPL probes, and LightCycler 480 Probes Master. All experiments were performed using biological duplicates and technical triplicates. Primer efficiencies were tested and selected for at least 1.80. The relative expression levels were calculated with real efficiencies.

Metabolomic Analysis

For embryos, 3 dpf embryos treated with vehicle or 5 μM Alfa for 24 hours were deyolked (11 per sample) and stored at -80°C. For hearts and livers, adult zebrafish were injected with vehicle or Alfa daily for 3 days and dissected 24 hours after the last injection before collecting hearts (4 per sample) and livers (2 per sample). All tissues were analyzed with 5 biological replicates and submitted for metabolite preparation and analysis to Duke University Proteomics and Metabolomics Core Facility. Each sample was sonicated, homogenized and processed using the AbsoluteIDQ p180 kit (Biocrates Innsbruck, Austria) according to manufacturer's protocol to prepare metabolites. Finally, metabolites were diluted and subjected to UPLC analysis (amino acids and biogenic amines) or flow injection analysis (acylcarnitines, sphingolipids, and glycerophospholipids).

QUANTIFICATION AND STATISTICAL ANALYSIS

Clutchmates were randomized into different treatment groups for each experiment. No animal or sample was excluded from the analysis unless the animal died during the procedure or deformed/destroyed due to fixation or dissection. All experiments were performed with at least two biological replicates, and at least 10 samples were used for each experiment unless otherwise indicated. All statistical values are displayed as Mean ± Standard Deviation. Statistics tests were calculated using two-tailed Student's t-tests when normality test was passed or Mann-Whitney Rank Sum test otherwise. ns, not significant, $*p < 0.05$, $**p < 0.01$; $*** p < 0.001$, $**** p < 0.0001$.

DATA AND SOFTWARE AVAILABILITY

The accession number for the RNA sequencing data reported in this paper is GEO database: GSE112826. All other relevant data are available from the corresponding author on request.